MUTUAL POUNDING OF ADJACENT STRUCTURES DURING EARTHQUAKES

J. P. WOLF, P. E. SKRIKERUD

Electrowatt Engineering Services Ltd.,
Bellerivestrasse 36, CH-8022 Zürich, Switzerland

Abstract

For adjacent structures separated by a small gap, there is a danger of their colliding in the event of a sufficiently large earthquake excitation. This mutual-pounding phenomenon has often caused extensive structural damage in past earthquakes. When retrofitting nuclear-power plants for increased seismic requirements, the size of the existing gap may be found to be too small. This can also arise when existing structures are recalculated with modern analytical procedures which account, e.g. for soil-structure interaction, including the material non-linearities of the soil and of the superstructure.

The consequences of the potential pounding have to be determined in order to be able to decide if the given structural configuration has to be altered or not. To examine the global response, the pounding structures are represented as simple spring-mass systems. Introducing an impact spring, which only acts in compression, leads to a non-linear dynamic system. Parametric studies are performed. The response for transient as well as for steady-state vibrations is compared to the corresponding linear results.

When the consequences of pounding are found to be unacceptable, the structural system has to be modified to reduce the response. Of the various ways of achieving this, the solution consisting of a spring-dashpot system between the two structures is examined parametrically.

By way of illustration, the response of a typical reactor building which is subjected to the pounding of an adjacent frame structure during an earthquake is determined. Relative displacements, stress resultants and in-structure response spectra are compared to those of the linear case, where the gap is sufficiently large. The comparison is also extended to the results obtained from aircraft impact.

For the harmonic excitation the well-known multiple solutions are observed when sweeping the frequency for constant amplitude as well as when increasing and decreasing the amplitude at a certain frequency. For real structures subjected to earthquake excitation, the influence of pounding has a minor effect on the overall response away from the zone of impact. However, in-structure response spectra are increased in the high-frequency range. Tuning reduces this magnification drastically. Nuclear structures can withstand a substantial amount of pounding, especially if they have been designed for the loading case of aircraft impact.

1. Introduction

For adjacent structures separated by a small gap, there is a danger of their colliding in the event of a sufficiently large earthquake excitation. This mutual-pounding phenomenon, which should be distinguished from the impact of collapsing structures, has often caused extensive structural damage in past earthquakes. For instance, the second story of a hospital hammered against its stairtower and the first floor banged against its neighbouring warehouse during the 1971 San Fernando Earthquake, because of insufficient width of the seismic joints [1]. These gaps can turn out to be too small in an actual severe earthquake, where plastic displacements of the soil and of the structure develop, as it is customary to design the structure for a moderate earthquake assuming elastic behavior. The problem of insufficient gap size can also arise when retro-fitting nuclear-power plants for increased seismic requirements or when recalculating them with modern analytical tools. The latter account for soil-structure interaction including possible uplift as well as the rotational-input component caused by traveling seismic waves.

In addition, pounding during earthquakes can also take place between a non-structural component and the structure itself as well as between two adjacent components. But pounding is not always a phenomenon which should be avoided by all means. For certain reactor-core structures, the pounding of the fuel rods is routinely accounted for in the design [2]. Recently, attempts have even been made to improve the seismic behavior of structures by introducing an additional stiffness which starts to act only when a certain displacement is reached [3, 4]. This "hardening spring" characteristic is analogous to that encountered in the analysis of pounding.

The consequences of the potential pounding have to be determined in order to be able to decide whether the given structural configuration has to be altered or not. As many nuclear structures are designed for missile impact, it is to be expected that a certain amount of pounding during earthquakes is acceptable. When the impact loads from pounding are too high, the structural system has to be modified to reduce the response [5]. This can be achieved, e.g.by tuning the two involved structures by introducing a spring dashpot system between them.

The complete paper will appear in the Journal "Nuclear Engineering and Design".

2. Vibroimpact of a One-Degree-of-Freedom System

To examine the global response of pounding structures, the one-degree-of-freedom system of Fig. 1 is studied first (mass m, stiffness k, damping coefficient c). The adjacent structure located at a distance e is represented by the impact mechanism consisting of a spring with stiffness k_e and of a damper with coefficient c_e. F_e denotes the impact force which acts when the displacement x relative to the ground motion x_g exceeds e. $I = \int F_e dt$ is the corresponding impulse (momentum). As the impact mechanism acts in compression only, a nonlinear dynamic model with a piecewise-linear (hardening) stiffness characteristic results. The following symbols are introduced: $\omega = \sqrt{k/m}$, $T = 2\pi/\omega$ and $\kappa = (k + k_e)/k$. The damping coefficient c_e is determined in such a way that the same damping ratio ξ also applies during impact ($\xi = c/2\sqrt{km} = (c + c_e)/2\sqrt{\kappa\, k\, m}$). For the special case of a rigid impact ($\kappa = \infty$), a coefficient of restitution ($= \exp(-\xi\pi)$) is introduced, which corresponds to the ratio of the velocities over half a cycle of the free vibration of a damped one-degree-of-freedom

oscillator. All results are obtained by numerical integration in the time domain, thus solving "rigorously" the governing equation of motion.

To gain insight into the nonlinear dynamic behavior, steady-state harmonic ground excitation with a circular frequency $\bar{\omega}$ and a displacement amplitude x_g is studied first. In Fig. 2, the well-known amplitude-response spectrum of the two-sided system (Fig. 1a)without damping is plotted for the parameters specified, for which analytical solutions exist [6, 7]. For increasing frequencies, the spectrum deviates from the corresponding linear one (i.e. without impact) when $|x|_{max}$ exceeds e. This also changes the natural frequency of the nonlinear system (dashed line) and the resonant response will thus be moved towards the value of $\sqrt{2}\cdot\omega$ (=2ω), which corresponds to the natural frequency of the system for amplitudes approaching infinity. For larger values of $\bar{\omega}/\omega$, the response drops sharply (accompanied by a phase shift of π) following the linear spectrum. For decreasing frequencies, this branch of the linear spectrum is followed until $|x|_{max}$ exceeds e, thus creating a frequency region of two solutions. For smaller frequency ratios, a jump to the increasing-frequency branch occurs*. The mathematically derivable continuation (dashed-dotted line) towards the nonlinear resonance frequency has no physical meaning, as it represents an instable solution. The amplitude-response spectrum when the gap size for the same system is varied, but with damping, is depicted in Fig. 3a. While the jump phenomenon again occurs when $|x|_{max}$ exceeds e (see $e/x_g = 3$), the drop for a damped system takes place when the response has reached a value corresponding approximately to that where the line connecting the resonant peaks of the two limiting linear cases ($e/x_g > 5$ and $e/x_g = 0$) intersects the curve describing the amplitude of free vibration (dashed line). For small values of e/x_g (see $e/x_g = 1$) the drop-jump phenomenon vanishes. Instead of sweeping the excitation frequency $\bar{\omega}$ for constant amplitude as in Fig. 3a, the same drop-jump phenomenon (for certain frequencies) is also observed when increasing and decreasing the amplitude x_g at a certain frequency (Fig. 3b).

The amplitude-response spectrum for harmonic ground excitation of the one-sided structural system (Fig. 1b), which is more relevant for pounding, is plotted for different values of κ in Fig. 4. For selected frequency ratios, the displacement-time histories are shown in Fig. 5 for $\kappa = \infty$. For the sake of simplicity, the gap size e = 0, which eliminates the linear of the two solutions present for the same frequency, as discussed above. The "natural circular frequency" of the nonlinear system varies from ω (κ = 1) to 2ω (κ = ∞). At this frequency, the familiar harmonic response peak whose value increases with κ, is visible in Fig. 4 (see also Fig. 5a). At twice (and integral multiples of, not shown in Fig. 4) the nonlinear natural frequency, the so-called subharmonic response develops which, for higher values of κ, is even larger than the corresponding harmonic response (Fig. 5b). Analogously, at half the nonlinear natural frequency, hyperharmonic responses (Fig. 5c) appear. For a frequency ratio lying in the intermediate range between harmonic and subharmonic response, a modest peak in the response spectrum occurs (Fig. 4). The corresponding displacements do not seem to be periodic (Fig. 5d). In Fig. 6 the in-structure (secondary) spectra of a linear oscillator subjected to the input motions depicted in Figs. 5a - c (solid lines) are plotted. For excitation frequencies $\bar{\omega}$ of the nonlinear structure (primary one-degree-of-freedom system) less than or equal to the nonlinear natural frequency 2ω (see curves $\bar{\omega}/\omega$=

*(with a phase shift of -π)

1 and 2), it is apparent that the maximum relative displacement occurs when the frequency of the secondary system coincides with the excitation frequency $\bar{\omega}$ (Fig. 6). In addition, at integral multiples of the excitation frequency ($2\bar{\omega}$, $3\bar{\omega}$ etc.) distinct peaks appear, which reflect the hyperharmonic response present in the displacement-time histories shown in the Figs. 5a and b. However, no subharmonic magnification is present. In contrast, for $\bar{\omega}$ greater than 2ω (see curve $\bar{\omega}/\omega = 4$ in Fig. 6 and Fig. 5c) a subharmonic response at $\bar{\omega}/2$ occurs, which leads to the largest spectral displacement of the secondary oscillator. Hyperharmonic peaks at multiples of this (subharmonic) frequency ($2 \cdot \bar{\omega}/2$, $3 \cdot \bar{\omega}/2$, etc.) are visible. In Figs. 7 and 8, the maximum impact force F_e and the transmitted impulse I per cycle of the excitation frequency, respectively, are plotted for the same cases as presented in Fig. 4.

Turning to transient ground excitation (x_g (t)), a 10-second artificial earthquake time-history (normalised to 1 g), whose response spectrum follows that of the USNRC Regulatory Guide 1.60, is used as input to the one-sided system of Fig. 1b. To stress the nonlinear behavior, $e = o$ and $\kappa = \infty$ are selected. In Fig. 9a, the maximum relative displacement x of the system is plotted as a function of ω together with the corresponding linear case (i.e. $\kappa = 1$). For frequencies above 0.2 Hz, the relative displacement, and thus also the global stress resultants, of the pounding structure are smaller than when no impact occurs. When comparing this remarkable result with the values for harmonic excitation shown in Fig.4, it should be noticed that in this figure ω appears in the denominator. This break-even frequency (0.2 Hz) depends heavily on the frequency content of the input-time history. This should be recognized when examining possible pounding of equipment located inside structures, as the latter will filter the time-history. In Fig. 9b, the input time-history is filtered by a linear one-degree-of-freedom system with a natural frequency of 1 Hz and a damping ratio of 0.07. This shifts the break-even frequency to 0.6 Hz. In Fig. 10, the (linear) in-structure spectra of the same one-sided system excited by the original time-history are represented (solid lines). The pounding-structural system has a linear natural frequency of 1 Hz. The in-structure response spectra for the same structure with no pounding are shown as dotted lines. As the nonlinear frequency of the pounding structure equals 2 Hz, the response curves (dashed lines) for a linear structure with the same natural frequency are drawn for comparison. The nonlinearity of the pounding structure is so pronounced that no relationship with the results of the original structure without pounding exists. The agreement is far better for the 2 Hz linear structure. The deviations caused by the sub- and hyperharmonics (see also Fig. 6) start at about 3 Hz (Fig. 10a). For the total accelerations (Fig. 10b) they are obviously more pronounced as the total acceleration of the pounding structure is infinite.

3. Pounding of a Frame Structure and an Adjacent Reactor Building

As a practical example, the hypothetical response of a reactor building which is subjected to the pounding of an adjacent frame structure (which forms part of the auxiliary building) during an earthquake is determined (Fig. 11). The frame structure is modeled as a simple one-degree-of-freedom system (mass m_a = 6.50 Gg, stiffness k_a = 3.14 GN/m, natural frequency 3.50 Hz). The axisymmetric reactor building is modeled with 32 curved higher-order isoparametric frusta in the meridional direction, leading to 297 degrees of freedom for

each of the 16 Fourier terms used circumferentially. The internal structures and the base mat are modeled as a rigid body. Consistent springs and dashpots are used for the discretization of the soil. For both structures a (modal) damping ratio of 0.07 is selected. The gap size e equals 17 mm. An impact area at Point B of 3.1 m in the meridional times 12.0 m in the circumferential direction is assumed. The impact-spring stiffness k_e equals the force required for a unit distortion of half of the horizontal frame slab k_{ea} = 30.0 GN/m. The impact-damping coefficient c_e (= c_{ea}) is determined in such a way that for the frame structure a damping ratio of 0.07 results when Point C is fixed.

In addition to this quite elaborate analysis, referred to as the "rigorous" solution further on, the pounding structures are also represented as a two-degree-of-freedom system (Fig. 12). While the modeling of the second structure is identical to that of the frame structure of Fig. 11 ($m_2 = m_a$, $k_2 = k_a$, $c_2 = c_a$), the properties of the first structure are associated with the response of the reactor building in the fundamental mode (2.30 Hz, first harmonic). This results in a generalized mass m_1 = 53.06 Gg, a generalized stiffness k_1 = 11.05 GN/m and c_1 = 0.107 GNs/m. The determination of the impact-spring stiffness k_e is illustrated in Fig. 11. In series to the spring with the stiffness k_{ea} of the frame structure, as already used in the rigorous analysis, a spring with stiffness k_{er} is connected, representing all modes with exception of the fundamental one. k_{er} equals the total force acting on the prescribed impact area for a resulting unit displacement calculated, omitting the contribution of the fundamental mode. With k_{er} = 2.74 GN/m, k_e is determined as 2.50 GN/m. For the two-degree-of-freedom system (when k_e is in operation) the average modal-damping ratio is selected as 0.07, thus determining c_e = 7.11 MNs/m. When the two pounding structures are tuned with a spring with stiffness k_t and a damper with coefficient c_t (Fig. 11), this spring is connected to the impact spring in series. This applies to the rigorous analysis and to the solution based on the two-degree-of-freedom system. c_e is determined analogously as in the case when no tuner is present. In the investigations, the same earthquake time-history as described in Section 2 is used, normalized to 0.3 g.

In Fig. 13, the relative-displacement time-histories at the impact Points B and C of the two pounding structures (without tuning) are shown for the rigorous analysis and for the two-degree-of-freedom model. An astonishing agreement results. This allows the simple two-degree-of-freedom model to be used for evaluating the appropriate tuning stiffness k_t (Fig. 14). The total impulse I transmitted during 10 s, the maximum impact force $F_{e\ max}$ and the maximum distortion $\delta_{t\ max}$ (= $(x_B - x_C)_{max}$) in the tuning spring k_t are plotted versus k_t. The optimum tuning stiffness (k_t = 1.85 GN/m) corresponds to the case of a completely distorted tuning spring (δ_t = e). For larger values of k_t, the corresponding I and $F_{e\ max}$ are significantly larger then when k_t = o.

The impact-force time-history F_e (t) is plotted in Fig. 15a, based on the rigorous analysis, with and without the optimum tuning device determined with the two-degree-of-freedom model. The tuning slightly reduces $F_{e\ max}$, considerably diminishes the high-frequency content in the force-time relationship (Fig. 15b), but, of course, increases the number of impacts and hence the total transmitted impulse (Fig. 14). The force-time relationship of a Boeing 707-320 impacting at a velocity of 103 m/s on a rigid wall [8] is shown for compari-

son. This impact force, which is used widely when hardening nuclear structures, is significantly larger than the pounding forces corresponding to a gap of 17 mm. This gap size is half the maximum relative displacement of Points B and C, based on a linear calculation of the two involved structures for the same earthquake excitation. In Fig. 16, the maximum meridional bending moments in the zone of impact are compared for the three cases for which the force-time relationships are plotted in Fig. 15a. In addition, results are also shown for the limiting case e = o, which also corresponds to a finite gap size with $k_t = \infty$ (Fig. 14). Again the loading case of aircraft impact dominates the design. The linear in-structure response spectra in Point A of the reactor building are compared in Fig. 17a for the earthquake load with and without pounding, and for the impacting aircraft [8]. As expected, the accelerations in the high-frequency range for the two impact-loading cases dominate those of the linear earthquake analysis. Once again, the aircraft impact is more stringent than the pounding. In Fig. 17b, the influence of tuning as well as the limiting case e = o is examined. As can be expected from the impact-force time-history (Fig. 15b), tuning reduces the high-frequency response. In Table I, the maximum response in selected points, based on the rigorous analysis is summarized. In Point B, the specified degrees correspond to the circumferential direction. It should be noted that the influence of pounding (with and without tuning as well as the limiting case e = o) has a minor effect on the overall response away from the zone of impact. The results obtained with the two-degree-of-freedom model (Table II) agree reasonably well with those obtained in the rigorous analysis (Table I).

References:

[1] S.A. Mahin et al: Response of the Olive View Hospital Main Building During the San Fernando Earthquake, EERC 76 - 22, University of California, Berkeley.

[2] A.J. Neylan and W. Gorholt: Design Development of the HTGR Core and its Support Structure - Seismic Considerations, Nuclear Engineering and Design, Vol. 29 (1974), pp. 231 - 242.

[3] L. Tzenov: Vibrations of a System with Joining Connections, 6th European Conference on Earthquake Engineering, Sept. 78, Paper 2 - 18.

[4] A. Poceski et al: Non-Stationary Bilinear Concept of Earthquake Resistant Design, 6th European Conference on Earthquake Engineering, Sept. 78, Paper 2 - 75.

[5] N.M. Newmark and E. Rosenblueth: Fundamentals of Earthquake Engineering, Section 15.8, Prentice Hall, 1971

[6] S. Timoshenko: Vibration Problems in Engineering, Chapter 2, Van Nostrand Reinhold, 1955.

[7] J.P. den Hartog and R.M. Heiles: Forced Vibration in Nonlinear Systems with Various Combinations of Linear Springs, Journal of Applied Mechanics, Vol. 3 (1936),

pp. 127 - 130.

[8] J.P. Wolf et al: Response of Equipment to Aircraft Impact, Nuclear Engineering and Design, Vol. 47 (1978), pp. 169 - 193.

Table I Maximum Response, Rigorous Analysis

		LINEAR	e=17mm	TUNING	e = o	BOEING
Horizontal Displacement at Point D	[mm]	72.6	71.7	73.9	73.7	15.6
Horizontal Displacement at Pont B, 0° x_B	[mm]	33.7	33.0	35.3	35.2	45.9
Horizontal Displacement at Point B, 90°	[mm]	33.2	33.0	33.4	33.3	10.4
Horizontal Displacement at Point B, 180°	[mm]	33.7	32.5	35.0	34.6	12.9
Horizontal Displacement of Reactor Base Mat	[mm]	11.6	11.5	11.7	11.8	1.8
Horizontal Displacement of Frame Building x_a	[mm]	15.7	13.4	13.9	15.9	---
Horizontal Acceleration at Point D	[g]	1.59	1.59	1.62	1.60	0.49
Horizontal Acceleration at Point B, 0° $\ddot{x}_B+\ddot{x}_g$	[g]	0.77	11.94	3.89	23.26	6.67
Horizontal Acceleration at Point B, 90°	[g]	0.76	0.99	0.85	1.16	0.95
Horizontal Acceleration at Point B, 180°	[g]	0.77	1.23	1.16	1.68	2.49
Horizontal Acceleration of Reactor Base Mat	[g]	0.78	0.77	0.78	0.79	0.10
Horizontal Acceleration of Frame Build. $\ddot{x}_a+\ddot{x}_g$	[g]	0.78	0.67	0.69	0.79	---
Global Overturning Moment of Reactor Building	[GN·m]	14.3	14.1	14.6	14.5	2.9
Impact Force F_e between Buildings	[MN]	0	36.0	24.9	42.3	88.3
Impulse I for First 10 s of Time History	[MN·s]	0	3.2	16.8	27.9	10.0

Table II Maximum Response, Two-Degree-of-Freedom System

		LINEAR	e=17 mm	TUNING	e = 0
Displacement x_1	[mm]	34.0	33.8	34.6	34.5
Displacement x_2	[mm]	15.6	14.9	15.6	20.0
Acceleration $\ddot{x}_1+\ddot{x}_g$	[g]	0.76	0.76	0.78	0.78
Acceleration $\ddot{x}_2+\ddot{x}_g$	[g]	0.78	0.74	0.77	0.99
Impact Force F_e	[MN]	0	34.4	30.6	61.8
Impulse I (first 10 s)	[MN·s]	0	4.2	17.5	28.0

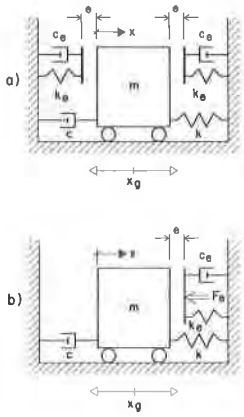

Fig. 1 Pounding Structure Modeled as a One-Degree-of-Freedom System: a) Two-Sided; b) One-Sided

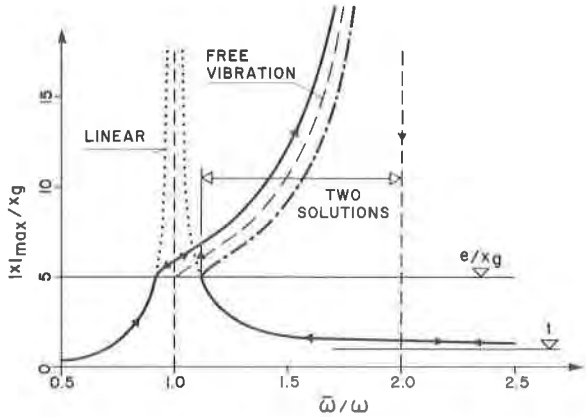

Fig. 2 Amplitude-Response Spectrum, Two-Sided System, $e/x_g = 5$, $\kappa = 4$, $\xi = 0$

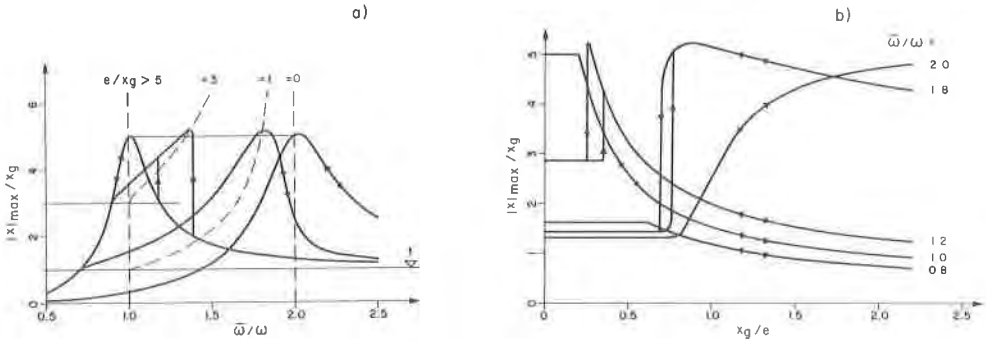

Fig. 3 Amplitude-Response Spectrum, Two-Sided System, $\kappa = 4$, $\xi = 0.1$: a) Frequency Sweep; b) Amplitude Sweep

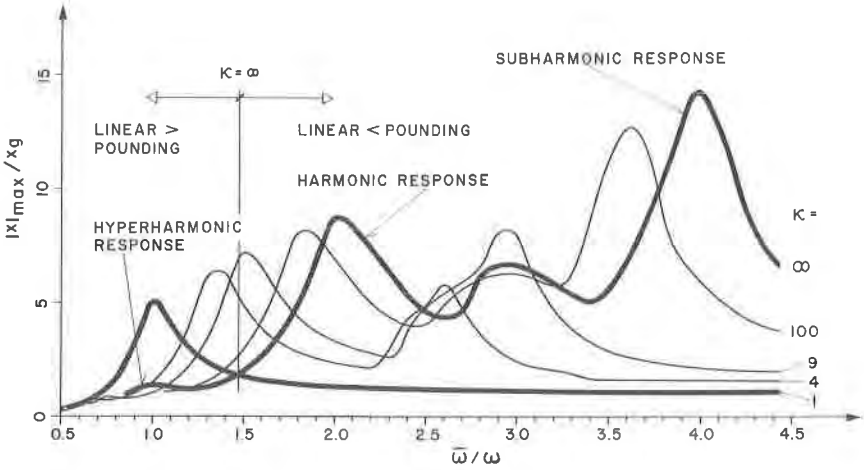

Fig. 4 Amplitude-Response Spectrum, One-Sided System, $e = 0$, $\xi = 0.1$

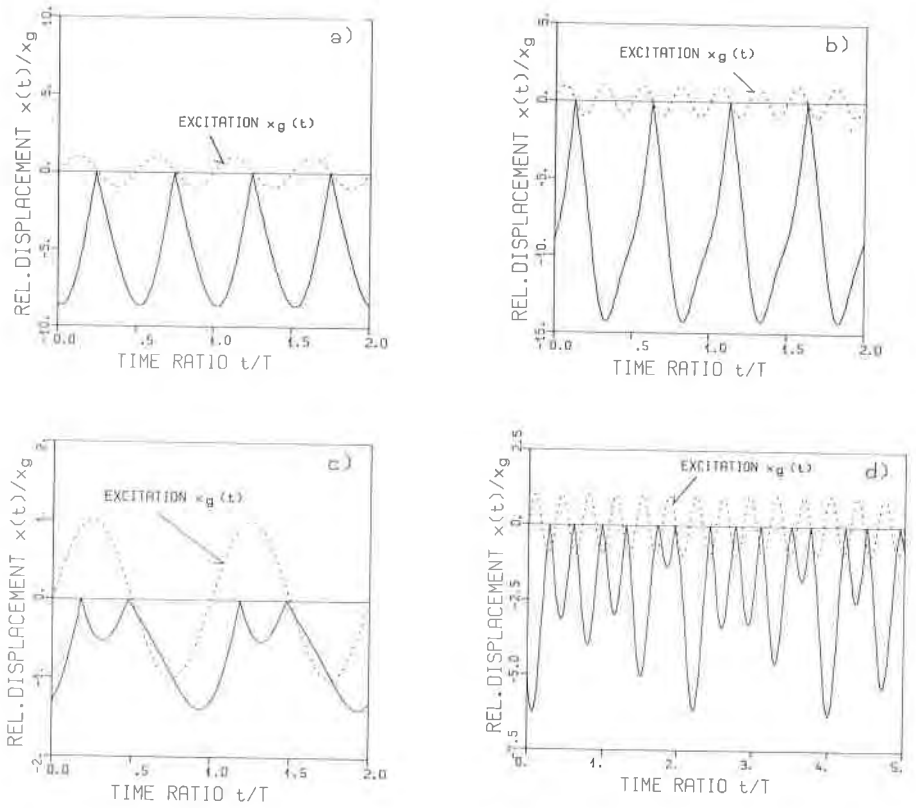

Fig. 5 Relative Displacement, Time-History, One-Sided System, e = 0, $\kappa = \infty$, $\xi = 0.1$: a) $\bar{\omega}/\omega = 2$, Harmonic Response; b) $\bar{\omega}/\omega = 4$, Subharmonic Response; c) $\bar{\omega}/\omega = 1$, Hyperharmonic Response; d) $\bar{\omega}/\omega = 2.8$, No Visible Periodicity

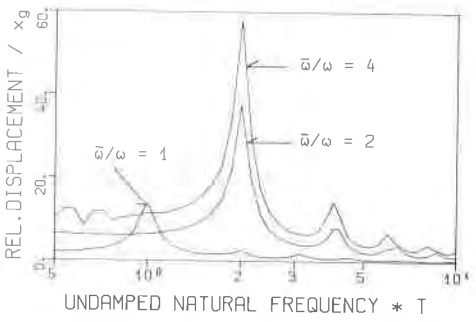

Fig. 6 (Linear) In-Structure Response Spectrum (5% Damping) of One-Sided System (e = 0, $\kappa = \infty$, $\xi = 0.1$)

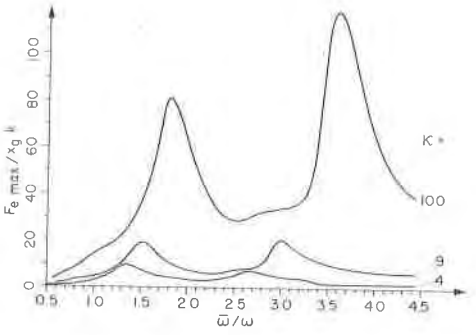

Fig. 7 Impact-Force Resonse Spectrum, One-Sided System, e = 0, $\xi = 0.1$

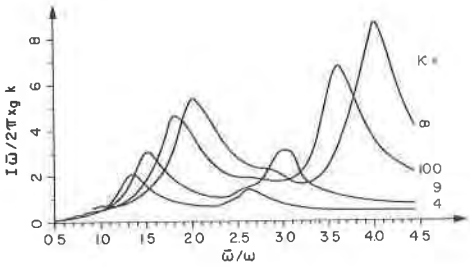

Fig. 8 Impulse-Response Spectrum, One-Sided System, $e = 0$, $\xi = 0.1$

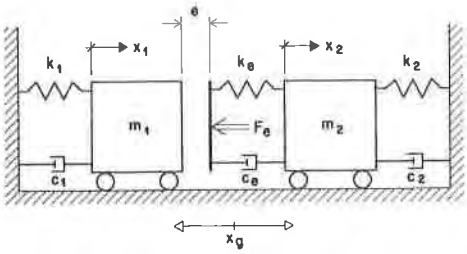

Fig. 12 Pounding Structures Modeled as a Two-Degree-of-Freedom System

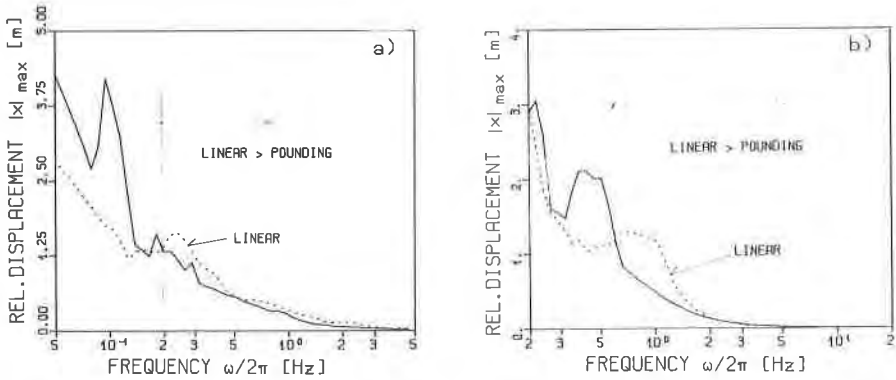

Fig. 9 Relative Displacement-Response Spectrum, One-Sided System, $e = 0$, $\kappa = \infty$, $\xi = 0.1$:
a) Original Time-History; b) Filtered Time-History (1 Hz, 7% Damping)

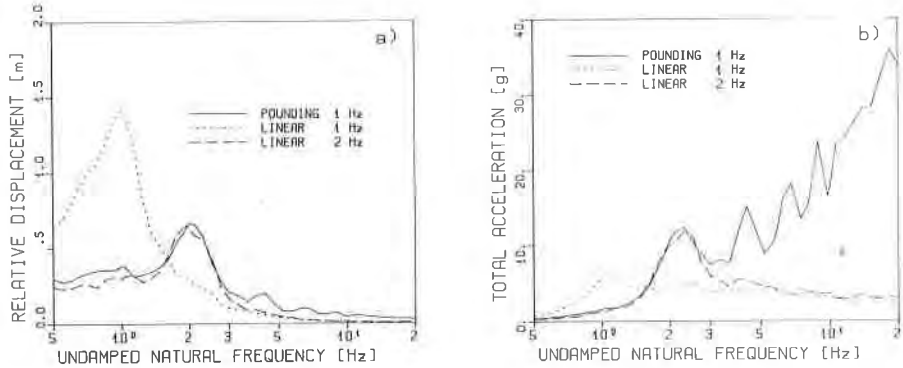

Fig. 10 (Linear) In-Structure Response Spectrum (5% Damping) of One-Sided System ($e = 0$, $\kappa = \infty$, $\xi = 0.1$), Original Time-History

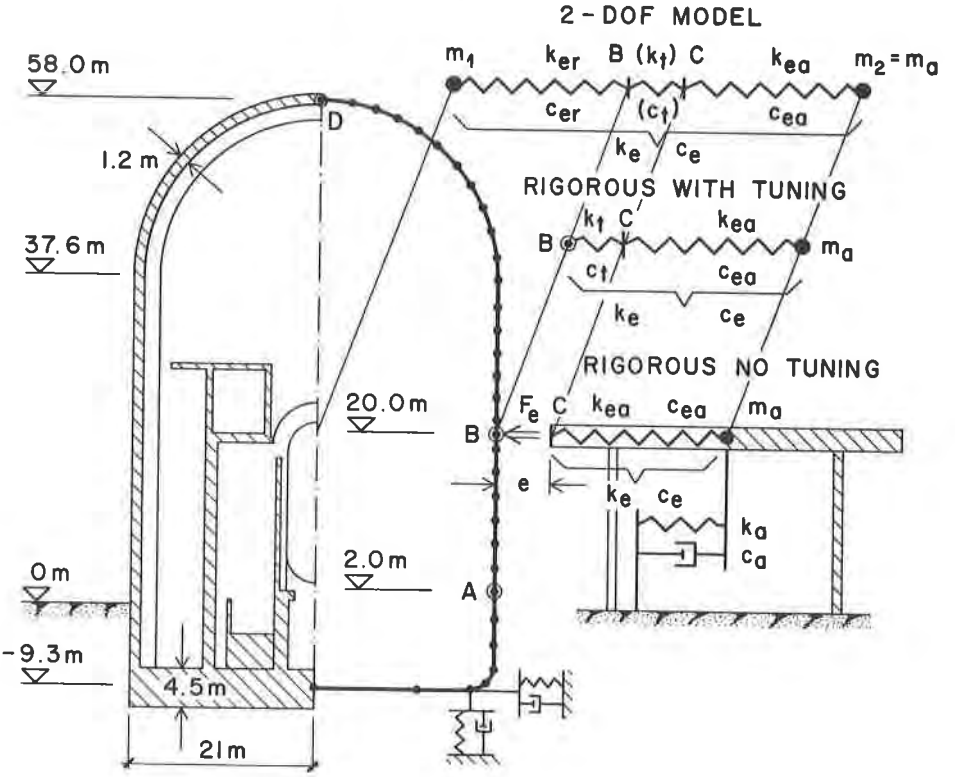

Fig. 11 Dynamic Model of Reactor Building and of Adjacent Frame Structure

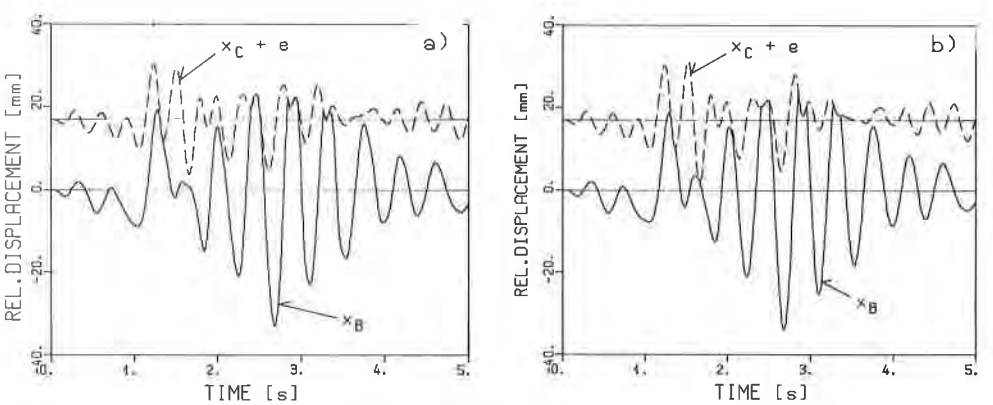

Fig. 13 Relative-Displacement Time-History: a) Rigorous Analysis; b) Two-Degree-of-Freedom System

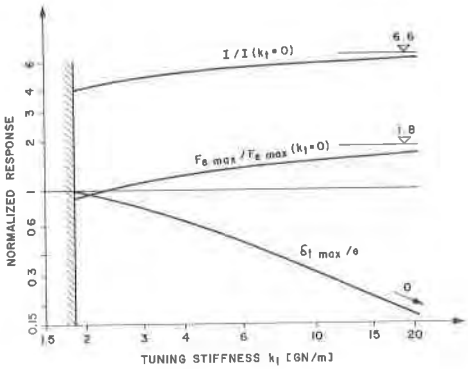

Fig. 14 Response of Two-Degree-of-Freedom System Versus Tuning Stiffness

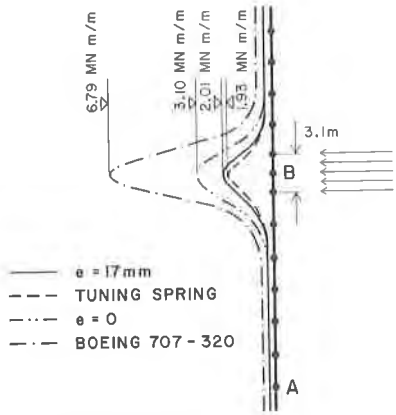

Fig. 16 Maximum Meridional Bending Moments in Zone of Impact of Reactor Building, Rigorous Analysis

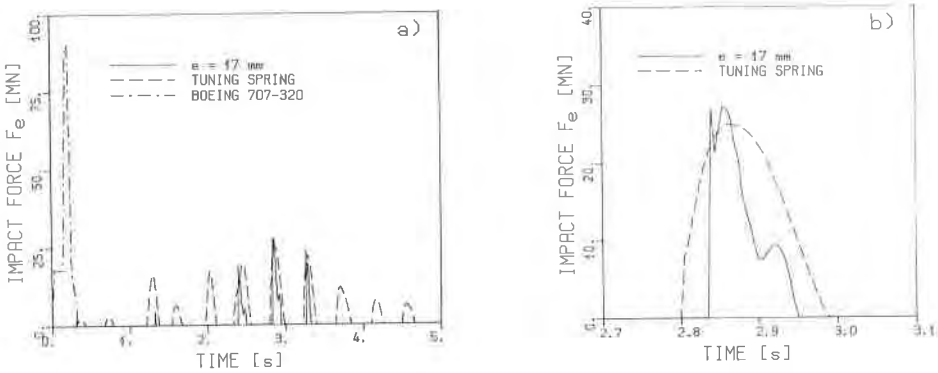

Fig. 15 Impact-Force Time-History, Rigorous Analysis: a) 5-second Record; b) Detail at 3 seconds

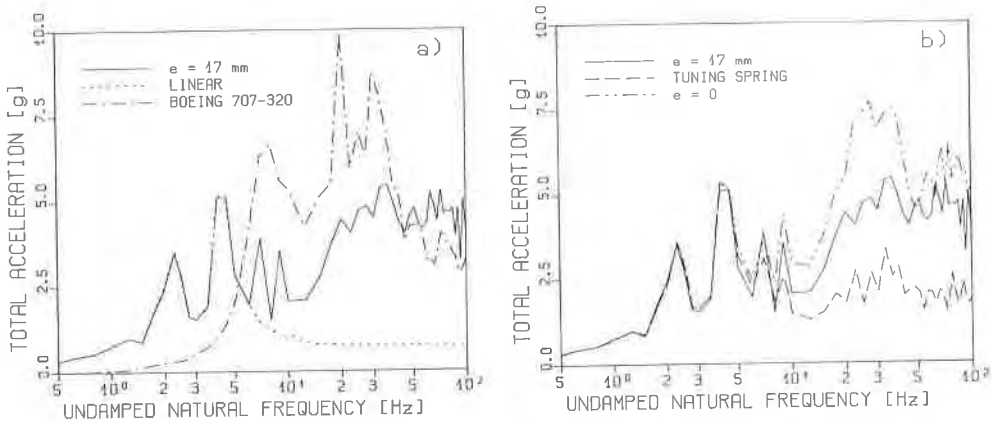

Fig. 17 (Linear) In-Structure Response Spectrum (1% Damping), Point A of Reactor Building, Rigorous Analysis